

Non-Gaussian two mode squeezed thermal states in continuous variable quantum teleportation

Chandan Kumar*

*Optics and Quantum Information Group, The Institute of Mathematical Sciences,
CIT Campus, Taramani, Chennai 600113, India. and*

Homi Bhabha National Institute, Training School Complex, Anushakti Nagar, Mumbai 400085, India.

While photon catalyzed two mode squeezed vacuum state has been considered in context of quantum teleportation, similar studies have not been yet conducted for photon catalyzed two-mode squeezed thermal (TMST) state. This can be attributed to challenges involved in the evaluation of teleportation fidelity for photon catalyzed TMST state. In this article, we consider a practical scheme for the implementation of non-Gaussian operation, viz., photon subtraction, photon addition, and photon catalysis, on TMST state. The generated states are employed as resources in continuous-variable quantum teleportation. The results show that the three non-Gaussian operations can enhance the teleportation fidelity. Considering the success probability of the non-Gaussian operations, we identify single-photon catalysis and single photon subtraction to be optimal for teleporting input coherent states, at low and intermediate squeezing levels.

I. INTRODUCTION

Squeezed states are an important nonclassical resource for continuous variable (CV) quantum information processing (QIP) [1, 2]. Generally pure squeezed states are preferable for quantum tasks; however, experimental imperfection and losses degrade the pure state to a mixed state [3]. These mixed states form an important family of mixed Gaussian states known as squeezed thermal states. Several studies characterizing single and multimode squeezed thermal states have been performed. For instance, photon statistics [4–6] and squeezing [7] have been investigated in such states. Reference [3] experimentally demonstrated teleportation of single-mode squeezed thermal state. Entanglement [8] and tomography [9] of two-mode squeezed thermal (TMST) state has also been undertaken. These states have found practical applications in diverse domains such as quantum teleportation [10], phase estimation [11–13], and quantum heat engine [14].

Non-Gaussian operations, namely, photon subtraction (PS), photon addition (PA) and photon catalysis (PC) have been considered on different states to ameliorate performance in various protocols such as quantum metrology [15–21] and quantum teleportation [22–28]. There exist other types of non-Gaussian operations such as coherent superposition operation of photon subtraction and addition [29] and number-conserving generalized superposition of products operation [30–32]; however, in this article, the term non-Gaussian operations shall refer to PA, PS, and PC operations only.

In the context of quantum teleportation, ideal photon-subtracted TMST (PSTMST) [33, 34] and ideal photon-added TMST (PATMST) [34, 35] states have been considered as resource states. However, the usefulness of photon catalyzed TMST (PCTMST) states in quantum

teleportation have not been examined. This is largely because of the complicated calculations involved in the evaluation of teleportation fidelity for PCTMST state.

Further, the ideal PS and PA operations are implemented via annihilation operator and creation operator, which is non unitary and thus cannot be implemented experimentally. In this article, we consider a practical scheme for the implementation of probabilistic non-Gaussian operations on TMST state [Fig. 1]. While PS and PA operations generate PSTMST and PATMST states, respectively, PC operation produces photon-catalyzed TMST (PCTMST) states. These three different family of states will be collectively referred as non-Gaussian TMST states. These states are used as resource states in teleporting input coherent and squeezed vacuum states. The analysis shows that while PS and PC operations can enhance the fidelity of teleporting input coherent state, PA operation does not. For the teleportation of input (highly) squeezed vacuum state, all three non-Gaussian operations can enhance fidelity.

The investigation also reveals that the fidelity via PS operation is optimized in the unit transmissivity limit, where the PSTMST state is basically reduced to the ideal PSTMST state. In unit transmissivity limit, the success probability of PS operation approaches zero, which is unsuitable from a practical point of view. Therefore, we trade-off between the enhancement in fidelity and success probability to find out the optimal non-Gaussian operation. To this end, we consider the product of fidelity enhancement and success probability. The result shows that single PC operation and single PS operation on TMST is the optimal operation at low and intermediate squeezing for the teleportation of input coherent states.

We stress that our practical scheme for the implementation of non-Gaussian operations can be implemented via currently available technology. The generation of multiphoton Fock state required in the considered practical scheme is feasible [36–40]. Further, photon number

* chandan.quantum@gmail.com

resolving detectors can also be implemented with existing technologies [41–43]. On a theoretical note, the derived Wigner characteristic function of the non-Gaussian TMST state is quite general including several parameters such as input multiphoton state, beam splitters transmissivity, and detected number of photons. This renders the calculation of Wigner characteristic function and fidelity a challenging task.

We arrange the rest of the paper as follow. In sec. II, we derive the Wigner characteristic function of the non-Gaussian TMST state. In Sec. III, we explore the advantages of non-Gaussian operations on TMST state in the teleportation of input coherent and squeezed vacuum states. In Sec. III C, We consider the success probability and identify optimal non-Gaussian operation. In Sec. V, we draw two-dimensional plots of success probability and fidelity enhancement to gain more insights. Sec. VI contains a summary of our results and mentions future directions. Appendix A contains a short description of CV system and phase space formalism.

II. DERIVATION OF THE WIGNER CHARACTERISTIC FUNCTION OF NON-GAUSSIAN TMST STATES

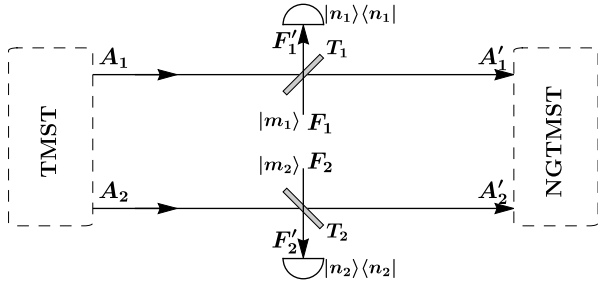


FIG. 1. Schematic for the generation of non-Gaussian two mode squeezed thermal state. Multiphoton states are mixed via beam splitters to each of the mode. Photon number resolving detectors are employed on both the modes for implementing non-Gaussian operations.

We discuss the implementation of non-Gaussian operations on the TMST state. The schematic is shown in Fig. 1. We start with a TMST state with modes labeled by A_1 and A_2 . A TMST state can be produced by operating two mode squeezing transformation on two uncorrelated thermal modes. The covariance matrix of two uncorrelated thermal modes is given by $V_{\text{th}} = (n_{\text{th}} + 1/2)\mathbb{1}_4$, where n_{th} is the average number of photons in a single mode thermal state. Therefore, the covariance matrix of the TMST state can be written as

$$V_{A_1 A_2} = S_{A_1 A_2}(r) V_{\text{th}} S_{A_1 A_2}(r)^T, \quad (1)$$

where $S_{A_1 A_2}(r)$ is the two mode squeezing transformation given by Eq. (A5) of the Appendix A. The covariance matrix of the TMSV state can be obtained by setting

$n_{\text{th}} = 0$ in Eq. (1). Since TMST state is a Gaussian state with zero mean and covariance matrix given by Eq. (1), the Wigner characteristic function of the TMST state can be readily evaluated using Eq. (A12):

$$\chi(\Lambda) = \exp \left[-\kappa(\tau_1^2 + \sigma_1^2 + \tau_2^2 + \sigma_2^2) \cosh(2r)/2 + \kappa(\tau_1 \tau_2 - \sigma_1 \sigma_2) \sinh(2r) \right], \quad (2)$$

where $\kappa = (n_{\text{th}} + 1/2)$. Further, modes F_1 and F_2 are initialized to Fock states $|m_1\rangle$ and $|m_2\rangle$. The four mode state can be represented via Wigner characteristic function formalism as

$$\chi_{F_1 A_1 A_2 F_2}(\Lambda) = \chi_{A_1 A_2}(\Lambda) \chi_{|m_1\rangle}(\Lambda_3) \chi_{|m_2\rangle}(\Lambda_4). \quad (3)$$

Now, mode A_1 (A_2) is mixed with mode F_1 (F_2), using a beam splitter of transmissivity T_1 (T_2) respectively. Consequently, the four modes get entangled. The four-mode entangled state is represented by

$$\chi_{F_1' A_1' A_2' F_2'}(\Lambda) = \chi_{F_1 A_1 A_2 F_2}(B(T_1, T_2)^{-1} \Lambda). \quad (4)$$

where $B(T_1, T_2) = B_{A_1 F_1}(T_1) \oplus B_{A_2 F_2}(T_2)$ denotes the collective action of the two beam splitters with $B_{ij}(T)$ being the beam splitter operation given in Eq. (A4) of the Appendix A. We employ photon number resolving detectors on the auxiliary modes F_1' and F_2' . When the detector in the output mode detects $|n_1\rangle$ and $|n_2\rangle$ photons, it heralds successful implementation of non-Gaussian operation on both the modes. The state after the measurement is given by

$$\begin{aligned} \tilde{\chi}_{A_1' A_2'}^{\text{NG}} = & \frac{1}{(2\pi)^2} \int d^2 \Lambda_3 d^2 \Lambda_4 \underbrace{\chi_{F_1' A_1' A_2' F_2'}(\Lambda)}_{\text{Four mode entangled state}} \\ & \times \underbrace{\chi_{|n_1\rangle}(\Lambda_3)}_{\text{Projection on } |n_1\rangle \langle n_1|} \underbrace{\chi_{|n_2\rangle}(\Lambda_4)}_{\text{Projection on } |n_2\rangle \langle n_2|}, \end{aligned} \quad (5)$$

which is unnormalized. If $m_i < n_i$, PS operation is performed on mode A_i . Similarly, if $m_i > n_i$ or $m_i = n_i$, PA or PC operation is performed on mode A_i . Performing PS, PA and PC operations on the TMST state leads to the generation of PSTMST, PATMST, and PCTMST states, respectively. We can perform non-Gaussian operations either on both modes or on a single mode of the TMST state. The former shall be referred to as symmetric (Sym) non-Gaussian operations, while the latter shall be referred to as asymmetric (Asym) non-Gaussian operations. Further, we set $m_1 = m_2 = 0$ for PS operation and $n_1 = n_2 = 0$ for PA operation. On integrating Eq. (5), we obtain

$$\tilde{\chi}_{A_1' A_2'}^{\text{NG}} = \hat{F}_1 \exp(\mathbf{\Lambda}^T M_1 \mathbf{\Lambda} + \mathbf{u}^T M_2 \mathbf{\Lambda} + \mathbf{u}^T M_3 \mathbf{u}), \quad (6)$$

where the column vectors $\mathbf{\Lambda}$ and \mathbf{u} are defined as $(\tau_1, \sigma_1, \tau_2, \sigma_2)^T$ and $(u_1, v_1, u_2, v_2, u_1', v_1', u_2', v_2')^T$ respectively, and the matrices M_1 , M_2 and M_3 are provided in Eqs. (B1), (B3) and (B5) of the Appendix B. Further,

the differential operator \widehat{F}_1 is given by

$$\widehat{F}_1 = \frac{2^{-(m_1+m_2+n_1+n_2)}}{m_1!m_2!n_1!n_2!} \frac{\partial^{m_1}}{\partial u_1^{m_1}} \frac{\partial^{m_1}}{\partial v_1^{m_1}} \frac{\partial^{m_2}}{\partial u_2^{m_2}} \frac{\partial^{m_2}}{\partial v_2^{m_2}} \quad (7)$$

$$\times \frac{\partial^{n_1}}{\partial u_1^{n_1}} \frac{\partial^{n_1}}{\partial v_1^{n_1}} \frac{\partial^{n_2}}{\partial u_2^{n_2}} \frac{\partial^{n_2}}{\partial v_2^{n_2}} \{\bullet\}_{u_1=v_1=u_2=v_2=0}.$$

Normalization of Eq. (6) yields the success probability of non-Gaussian operations and can be calculated as

$$P^{\text{NG}} = \widetilde{\chi}_{A_1' A_2'}^{\text{NG}} \Big|_{\tau_1=\sigma_1=\tau_2=\sigma_2=0} = \widehat{F}_1 \exp(\mathbf{u}^T M_3 \mathbf{u}). \quad (8)$$

Therefore, the normalized Wigner characteristic function $\chi_{A_1' A_2'}^{\text{NG}}$ of the non-Gaussian TMST states turns out to be

$$\chi_{A_1' A_2'}^{\text{NG}}(\tau_1, \sigma_1, \tau_2, \sigma_2) = (P^{\text{NG}})^{-1} \widetilde{\chi}_{A_1' A_2'}^{\text{NG}}(\tau_1, \sigma_1, \tau_2, \sigma_2). \quad (9)$$

We can obtain the Wigner characteristic function of several special states from Eq. (9). The Wigner characteristic function of the ideal PSTMST state $\mathcal{N}_s \hat{a}_1^{n_1} \hat{a}_2^{n_2} |\text{TMST}\rangle$ is obtained in the unit transmissivity limit $T_1 \rightarrow 1$ and $T_2 \rightarrow 1$ with $m_1 = m_2 = 0$. Here \mathcal{N}_a is the normalization factor. Similarly, the Wigner characteristic function of the ideal PATMST state $\mathcal{N}_s \hat{a}_1^{\dagger m_1} \hat{a}_2^{\dagger m_2} |\text{TMST}\rangle$ is obtained in the unit transmissivity limit $T_1 \rightarrow 1$ and $T_2 \rightarrow 1$ with $n_1 = n_2 = 0$. Here \mathcal{N}_s is the normalization factor. Further, the Wigner characteristic function of the non-Gaussian TMSV state can be obtained by setting $\kappa = 1/2$ (equivalently $n_{\text{th}} = 0$) in Eq. (9).

III. ADVANTAGES OF NON-GAUSSIAN OPERATIONS ON TMST STATE IN CV QUANTUM TELEPORTATION

We now analyze the teleportation of input coherent and squeezed vacuum states using non-Gaussian TMST resource states. We first briefly describe the BK protocol [44] that can be used to teleport an unknown input quantum state between two parties, from Alice to Bob. The implementation of this protocol prerequisites a shared pair of entangled states between the two parties. In order to teleport an unknown single-mode quantum state, Alice uses a balanced beam splitter to combine the input quantum state with her mode of the resource state and subsequently subjects the two output modes to homodyne measurements. The results of these measurements are then communicated by Alice to Bob through a classical channel. As per the results obtained in the measurements, Bob appropriately displaces the mode in his possession in order to retrieve the initial input state. The success of this protocol can be characterized using fidelity F , given by,

$$F = \text{Tr}[\rho_{\text{in}} \rho_{\text{out}}] \quad (10)$$

where ρ_{in} and ρ_{out} denote the density operator of the input state and the output state, respectively. In

the Wigner characteristic function formalism, where the Wigner characteristic functions of the input and output states are respectively given by $\chi_{\text{in}}(\Lambda_2)$ and $\chi_{\text{out}}(\Lambda_2)$, the fidelity can be computed through the following integral:

$$F = \frac{1}{2\pi} \int d^2 \Lambda_2 \chi_{\text{in}}(\Lambda_2) \chi_{\text{out}}(-\Lambda_2), \quad (11)$$

where the output state $\chi_{\text{out}}(\Lambda_2) \equiv \chi_{\text{out}}(\tau_2, \sigma_2)$, can be expressed as a product function of the Wigner characteristic function of the input state and the entangled resource state:

$$\chi_{\text{out}}(\tau_2, \sigma_2) = \chi_{\text{in}}(\tau_2, \sigma_2) \chi_{A_1' A_2'}(\tau_2, -\sigma_2, \tau_2, \sigma_2), \quad (12)$$

It is a known result that the fidelity of teleporting a coherent state cannot exceed the value of 1/2 when only classical resources are utilized [45, 46]. Therefore, a fidelity value above 1/2 indicates the usage of quantum resources.

A. Teleporting an input coherent state using non-Gaussian TMST resource states

Having described the BK protocol for CV quantum teleportation, we now consider the teleportation of input coherent state. To evaluate the fidelity, we use the Wigner characteristic function of the non-Gaussian TMST resource states (9) and coherent state (A12). The expression of fidelity can be evaluated using Eq. (11). We proceed to analyze the fidelity of teleporting input coherent state using non-Gaussian TMST resource states with respect to squeezing and thermal parameters.

While analyzing the fidelity as a function of the squeezing parameter, we consider a fixed low value of thermal parameter $\kappa = 0.51$ to make the fidelity curves for different non-Gaussian TMST states distinguishable. Different fidelity curves coincide for higher κ values and therefore are difficult to distinguish¹.

We perform numerical optimization to maximize the fidelity by adjusting the transmissivity of the beam splitters. The results of this optimization are presented in Fig. 2. We observe that Sym PS operations enhance the teleportation fidelity of the TMST state. However, Asym PS operations are detrimental to quantum teleportation. We also see that neither Asym nor Sym PA operation enhances the teleportation fidelity. The analysis of Sym PC operation reveals that it can enhance the fidelity till a certain squeezing threshold r_{th} . Beyond this threshold squeezing, the fidelity is optimized at unit transmissivity. Since the PCTMST state becomes the TMST state in unit transmissivity limit, the fidelity beyond r_{th} for the PCTMST state is equal to that of the

¹ We explore the fidelity dependence on κ in Sec. IV.

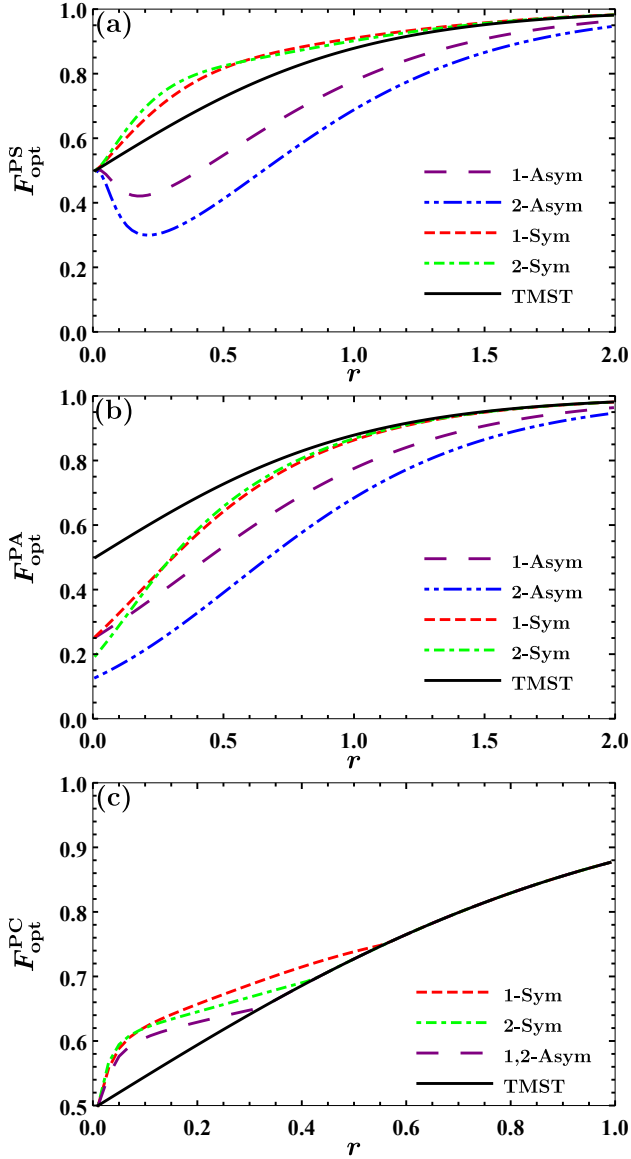


FIG. 2. Optimized fidelity for teleporting input coherent state as a function of the squeezing parameter r for (a) PSTMST states, (b) PATMST states, and (c) PCTMST states with $\kappa = 0.51$. We have adjusted the transmissivities of the beam splitters to maximize the fidelity.

TMST state. While performing PC operation on one mode is undesirable, we also see that Asym 1,2-PC operation ($m_1 = n_1 = 1$ and $m_2 = n_2 = 2$) is beneficial.

We observe a major difference between the fidelity results for PC operation on TMST and TMSV [27] states. While the optimized fidelity for Sym 1-PCTMSV state exhibits a jump as the squeezing transitions from zero to non-zero values, no such characteristic is observed for Sym 1-PCTMST state.

To get a precise idea of the magnitude of enhancement and the optimal squeezing and transmissivity, we can consider a new figure of merit termed fidelity en-

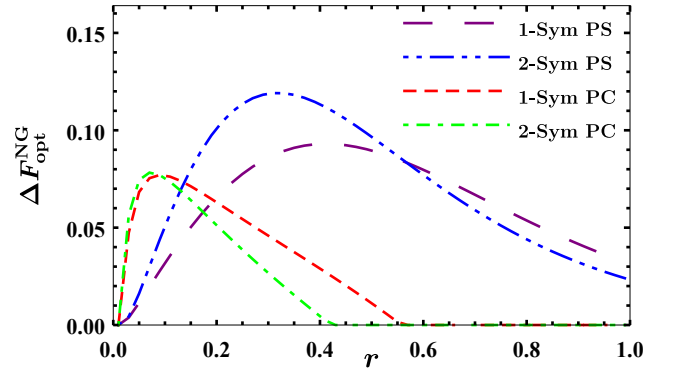


FIG. 3. Optimized fidelity enhancement, $\Delta F_{\text{opt}}^{\text{NG}}$, as a function of the squeezing parameter r with $\kappa = 0.51$. We have adjusted the transmissivities of the beam splitters to maximize $\Delta F_{\text{opt}}^{\text{NG}}$.

hancement defined as follows:

$$\Delta F^{\text{NG}} = F^{\text{NG}} - F^{\text{TMST}}. \quad (13)$$

We optimize ΔF^{NG} with respect to transmissivity and present the results in Fig. 3. We see that the enhancement rendered by Sym PS operations surpasses the Sym PC operations. Further, the 2-Sym PS operation demonstrates superior performance when compared to the 1-Sym PS operation. On the other hand, both the 1-Sym and 2-Sym PC operations exhibit nearly identical performance.

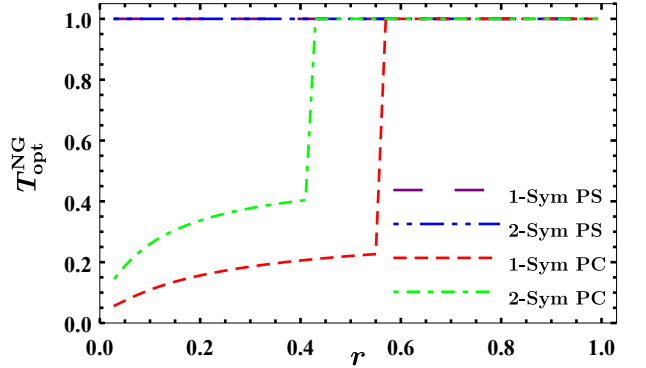


FIG. 4. The optimal beam splitter transmissivities, that maximize F^{NG} (Fig. 2) or ΔF^{NG} (Fig. 3).

The optimal transmissivity values for Figs. 2 and 3 are identical and are depicted in Fig. 4. The results reveal that the optimal transmissivity for PS operation is unity, and therefore the corresponding fidelity results are identical to those of the ideal PSTMST states. Similarly, the fidelity for the PATMST state is optimized in unit transmissivity limit (not shown in Fig. 4) and hence the results are identical to those of the ideal PATMST state. For the PC operation, the optimal transmissivity lies below 1/2 until a certain threshold squeezing value, denoted

as r_{th} , beyond which the optimal transmissivity becomes unity. It is worth mentioning that previous works, such as Refs. [33–35] have already investigated quantum teleportation employing ideal PSTMST and PATMST resource states.

B. Teleporting an input squeezed vacuum state using non-Gaussian TMST resource states

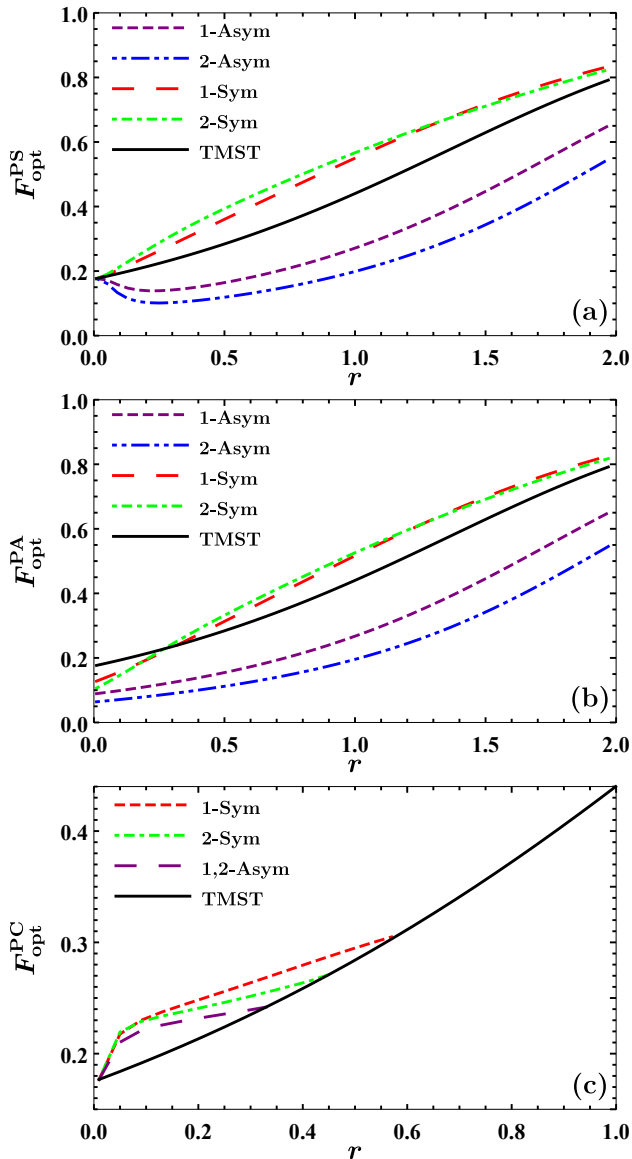


FIG. 5. Optimized fidelity as a function of the squeezing parameter r for (a) PSTMST states, (b) PATMST states, and (c) PCTMST states for $\kappa = 0.51$. The state to be teleported is input squeezed vacuum state with $\epsilon = 1.7$. We have adjusted the transmissivities of the beam splitters to maximize the fidelity.

We now consider the teleportation of an input squeezed

vacuum state with squeezing ϵ , whose Wigner characteristic function is provided in Eq. (A14). The expression of fidelity can be evaluated using the expression of fidelity (11). For our analysis, we choose the squeezing of the input vacuum state to be $\epsilon = 1.7$, which is the maximum squeezing achieved experimentally up until now [47]. We maximize the fidelity by adjusting the transmissivity of the beam splitters and present the results in Fig. 5. The fidelity curves corresponding to PS and PC operations display similar behavior to that was observed for the teleportation of an input coherent state (Fig. 2). However, we observe that Sym PA operations on the TMST state can also enhance the fidelity. This result is contrary to the earlier observation of teleportation of an input coherent state.

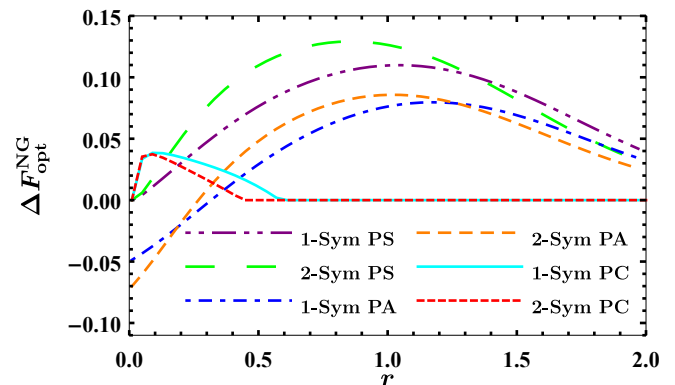


FIG. 6. Optimized fidelity enhancement $\Delta F_{\text{opt}}^{\text{NG}}$, as a function of the squeezing parameter r with $\kappa = 0.51$. The state to be teleported is input squeezed vacuum state with $\epsilon = 1.7$. We have adjusted the transmissivities to maximize $\Delta F_{\text{opt}}^{\text{NG}}$.

To identify the optimal values of squeezing and transmissivity that yield maximum advantage, we employ fidelity enhancement as a figure of merit. The results are shown in Fig. 6. We observe that PS operations offer the greatest advantage, followed by PA operations. However, at low squeezing, PC operations provide the highest advantage.

We plot the transmissivity maximizing the fidelity (or fidelity enhancement) in Fig. 7. The trend observed in the optimal transmissivity closely aligns with that of coherent state teleportation (Fig. 6). The optimal transmissivity for the PS and PA operation turns out to be unity, resulting in what we term as ideal PSTMST and ideal PATMAST states. These states have been employed as resource states for teleportation of input squeezed vacuum state in Ref. [34].

C. Success probability and optimal non-Gaussian operation

As stated in Sec. II, the considered non-Gaussian operations exhibit a probabilistic nature, with their proba-

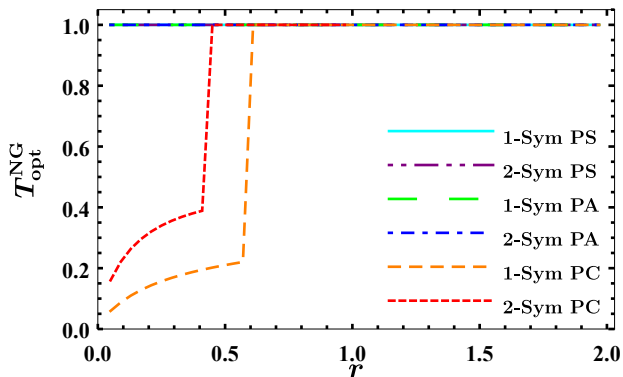


FIG. 7. The optimal beam splitter transmissivities, that maximize F^{NG} (Fig. 5) or ΔF^{NG} (Fig. 6).

bility being determined by Eq. (8). In our previous analysis, our primary focus was to maximize the fidelity by adjusting the transmissivity without considering success probability. To emphasize the significance of considering success probability, let us examine the case of 1-PSTMST state. It was observed that the fidelity is maximized in the unit transmissivity limit. However, in this particular limit, the success probability approaches zero. This scenario is highly undesirable from a practical point of view.

To obtain optimal conditions, we trade off between the enhancement in fidelity ΔF^{NG} and success probability by adjusting the transmissivity. To perform a thorough quantitative analysis, we examine the product $\mathcal{R}^{\text{NG}} = \Delta F^{\text{NG}} \times P^{\text{NG}}$. We aim to find its maximum value and the corresponding values of squeezing and transmissivity. We have shown the results in Table I for the teleportation of input coherent states. On comparing with Fig. 3, the magnitude of ΔF^{NG} has reduced from 9.3×10^{-2} to 3.3×10^{-2} for the 1-PSTMST state. However, the success probability, which tends to zero in the unit transmissivity limit, is now of the order 10^{-2} – a practically reasonable value. It is worth mentioning that an experimental demonstration of single PS operation with an even lower probability (of the order 10^{-5}) has been conducted [48].

For a visual perspective, we plot the product \mathcal{R}^{NG} as a function of transmissivity for different non-Gaussian TMSV and non-Gaussian TMST states at optimal squeezing in Fig. 8. We observe that while the PC operation is optimal at low squeezing, the PS operation is optimal at intermediate squeezing. We can verify the numerical values of different quantities in Fig. 8 with numerical values given in Table I.

In the next section, we delve into an exploration of how the fidelity varies with the thermal parameter.

TABLE I. The maximum value of the product $\mathcal{R}^{\text{NG}} = \Delta F^{\text{NG}} \times P^{\text{NG}}$ and magnitude of the other quantities at optimal squeezing and transmissivity.

States	1-PSTMST	1-PSTMSTV	1-PCTMST	1-PCTMSTV
$\mathcal{R}_{\text{max}}^{\text{NG}}$	8.2×10^{-4}	9.5×10^{-4}	2.2×10^{-3}	2.9×10^{-3}
r_{opt}	0.64	0.64	0.24	0.26
T_{opt}	0.78	0.77	0.18	0.18
F^{NG}	0.81	0.82	0.66	0.70
ΔF^{NG}	3.3×10^{-2}	3.7×10^{-2}	5.5×10^{-2}	7.1×10^{-2}
P^{NG}	2.5×10^{-2}	2.6×10^{-2}	4.0×10^{-2}	4.1×10^{-2}

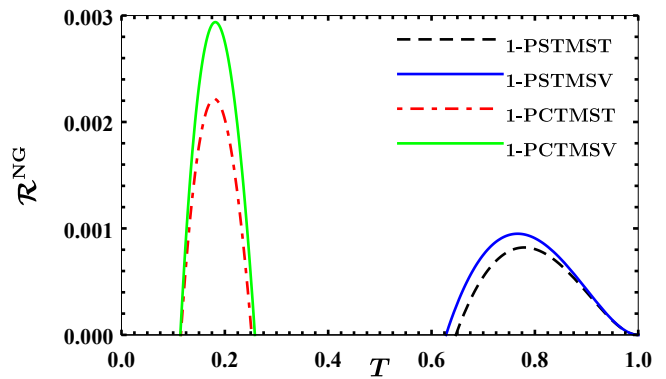


FIG. 8. Product $\mathcal{R}^{\text{NG}} = P^{\text{NG}} \times \Delta F^{\text{NG}}$ as a function of the transmissivity T for different non-Gaussian TMST and non-Gaussian TMSV states for teleportation of input coherent states. We have taken $\kappa = 0.51$ for non-Gaussian TMST states and the optimal squeezing value is considered (Table I). Further, we have considered symmetric non-Gaussian operations.

IV. VARIATION OF FIDELITY WITH THERMAL PARAMETER κ

In the earlier analysis, we have set the thermal parameter $\kappa = 0.51$. In this section, we study the variation of the fidelity with κ . We plot the optimized fidelity for teleporting input coherent states as a function of κ for PSTMST and PCTMST states in Fig. 9. We observe that both Sym 1-PS and Sym 2-PS operations can enhance the fidelity in the initial range of the thermal parameter. Moreover, we also notice that Sym 2-PS operation can enhance the fidelity for $\kappa \gtrsim 0.95$. The corresponding optimal transmissivity for 2-PS operation turns out to be zero. In this region, the numerical value of the fidelity is equal to 1/2.

In the case of PC operation, the fidelity for PCTMST states surpasses that of the TMST state in the initial thermal parameter range. This is followed by a narrow thermal parameter region where the fidelity of the PCTMST states matches that of the TMST state. In this narrow region, the optimal transmissivity is unity,

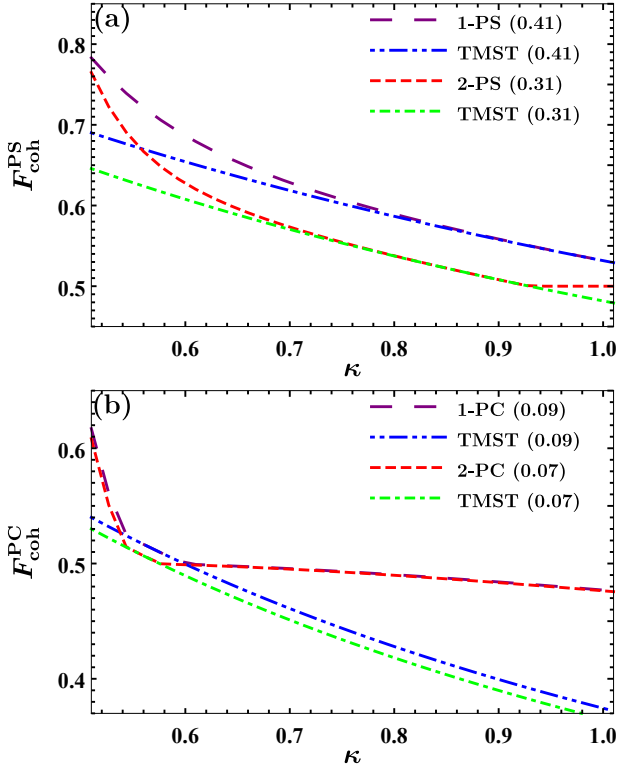


FIG. 9. Optimized fidelity for teleporting input coherent state as a function of the thermal parameter κ for (a) PSTMST states, and (b) PCTMST states. The optimal squeezing r has been set in accordance with Fig. 3. We have adjusted the transmissivities of the beam splitters to maximize the fidelity. We note that we have considered symmetric non-Gaussian operations.

where the PCTMST states are basically the TMST state. As the thermal parameter increases, the PCTMST states consistently outperform the TMST state in terms of fidelity. However, within this particular region, the fidelity falls below the threshold of $1/2$, thereby demonstrating that quantum resources are not useful.

Nevertheless, within this particular domain, it is worth noting that the fidelity falls below the threshold of $1/2$, thereby exemplifying the limited utility of quantum resources in this context.

Now let us focus on the scenario where we teleport input squeezed vacuum states and conduct a similar analysis. The results of this analysis are shown in Fig. 10. The fidelity trends for both PS and PC operations are more or less similar to those observed in the case of input coherent state teleportation. However, the PS operation can enhance the fidelity for a larger range of thermal parameter range as compared to the case of input coherent state teleportation. Additionally, we note that PA operation can enhance the fidelity within the considered range of the thermal parameter. As depicted in Fig. 11(b), the optimal transmissivity associated with PS and PC operations in the context of teleporting input squeezed vacuum

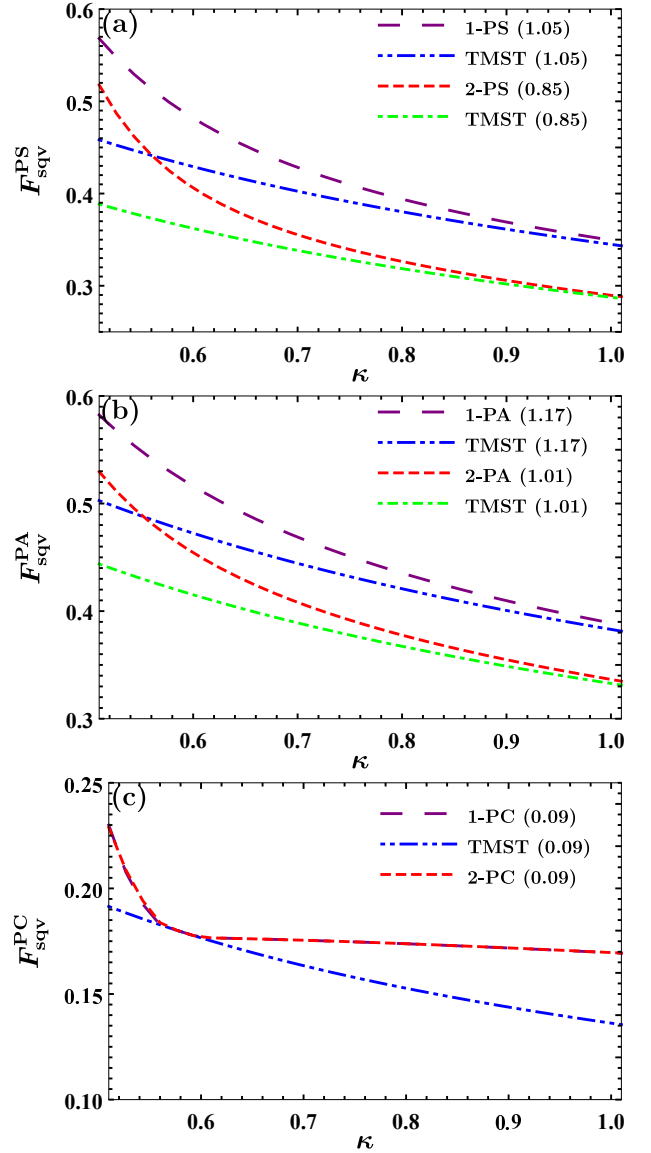


FIG. 10. Optimized fidelity for teleporting input squeezed vacuum state as a function of the thermal parameter κ for (a) PSTMST states, (b) PATMST states, and (c) PCTMST states. The optimal squeezing r has been set in accordance with Fig. 6. We have set the squeezing of the input squeezed vacuum state $\epsilon = 1.7$. We have adjusted the transmissivities of the beam splitters to maximize the fidelity. The value of squeezing is provided in parentheses. We note that we have considered symmetric non-Gaussian operations.

states follows a similar pattern to that observed in the teleportation of input coherent states (Fig. 11(a)). Furthermore, the optimal transmissivity for PA operations is unity.

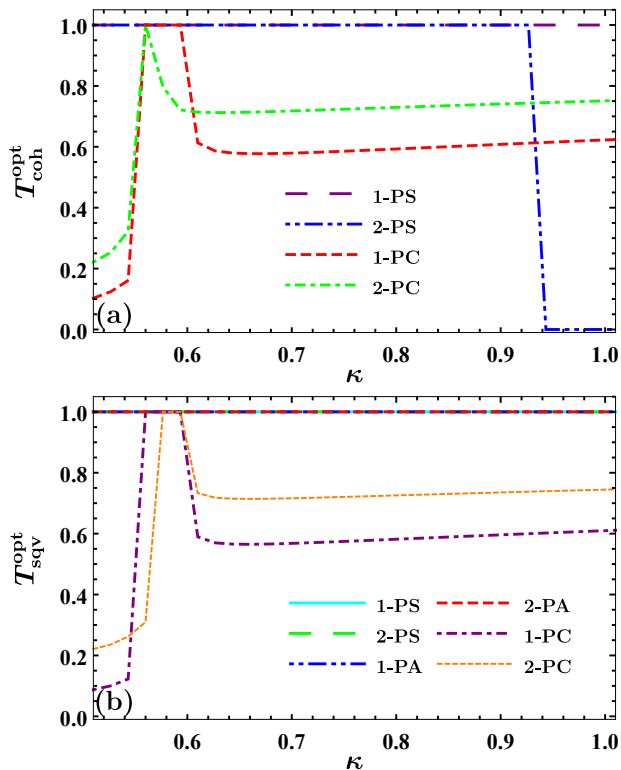


FIG. 11. Optimal transmissivity as a function of the thermal parameter κ for (a) teleportation of input coherent states, and (b) teleportation of input squeezed vacuum states.

V. TWO DIMENSIONAL PLOT OF SUCCESS PROBABILITY AND FIDELITY ENHANCEMENT

We now analyze the advantageous non-Gaussian resource states namely 1-PSTMST and 1-PCTMST states for teleporting input coherent state using two-dimensional plots. This approach provides us insightful observations about the magnitude of success probability and fidelity enhancement ΔF^{NG} for different squeezing and transmissivity values.

To see the effects of thermal parameter, we first carry out the analysis for NGMTSV states (special case of non-Gaussian TMST states obtained for $\kappa = 1/2$) and present the results in Fig. 12.

In the first column, we depict the success probability of different non-Gaussian operations. We note that the maximum success probability attainable for PS operation is less than PC operation. In the second column, the fidelity enhancement ΔF^{NG} for teleporting input coherent state is shown. Gray shaded region corresponds to $\Delta F^{\text{NG}} > 0$ with $F > 1/2$. For squeezing and transmissivity in the gray shaded parameter region, it is advantageous to perform non-Gaussian operations. A detailed quantitative analysis for non-Gaussian TMSV states can be found in Ref. [27].

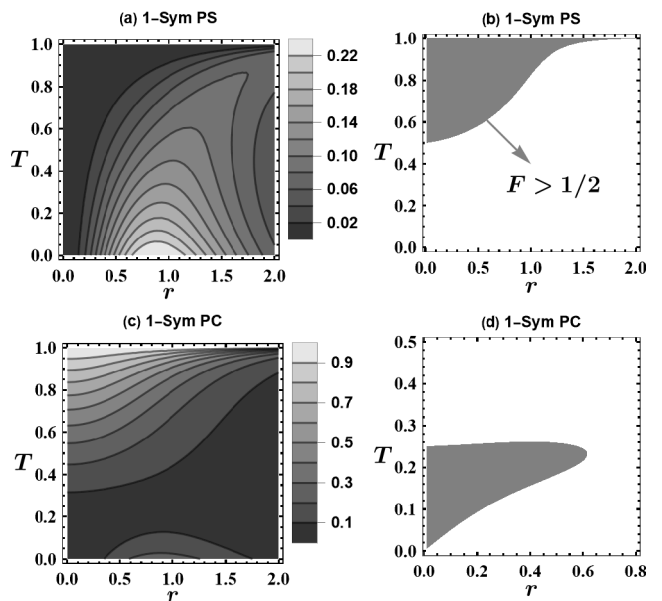


FIG. 12. First column: Success probability of different non-Gaussian operations on the TMSV state. Second column: Fidelity enhancement ΔF^{NG} for the teleportation of input coherent states using different non-Gaussian TMSV resource states. Gray shaded region corresponds to $\Delta F^{\text{NG}} > 0$ with $F > 1/2$.

We shall now embark upon the examination of the success probability and fidelity enhancement rendered by the non-Gaussian TMST states. We present the results in Figs. 13 and 14 for $\kappa = 3/4$ and 1, respectively. We note that the magnitude of success probability of non-Gaussian operations on TMST states is reduced as compared to non-Gaussian operations on TMSV states.

We now discuss the fidelity enhancement ΔF^{NG} for the teleportation of input coherent state. In addition to the gray shaded region, we see the appearance of black shaded region corresponds to $\Delta F^{\text{NG}} > 0$ but $F < 1/2$. We see that a vertical straight line along the transmissivity ordinate divides the black shaded region to the other parameter region.

Here, we offer an explanation for the emergence of straight lines and $F < 1/2$ in the case of the PSTMST state (Figs. 13(b) and 14(b)). The classical nature of the TMST state persists until the condition $e^{-2r}\kappa < 1/2$ is satisfied. Specifically, for $\kappa = 3/4$ and 1, the TMST state is a classical state when r is less than 0.20 and 0.35, respectively. Since a PS operation is incapable of transforming a classical state into nonclassical state [49], the teleportation fidelity via classical resource state remains lower than 1/2.

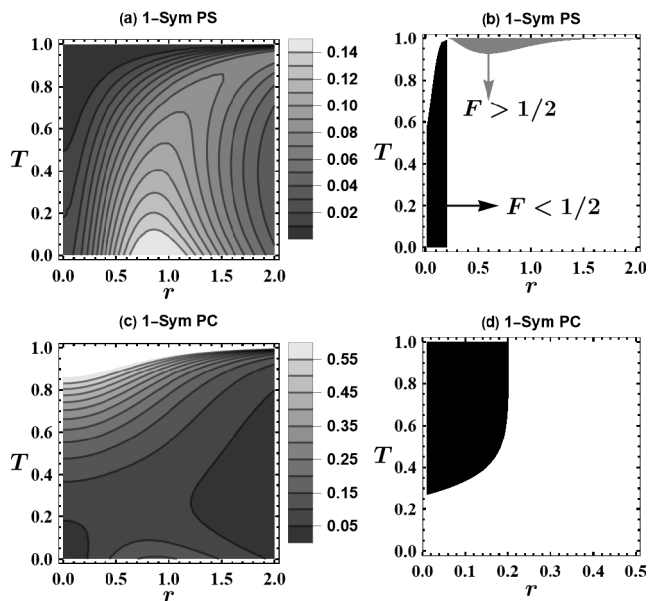


FIG. 13. First column: Success probability of different non-Gaussian operations on the TMST state. Second column: Fidelity enhancement ΔF^{NG} for the teleportation of input coherent states using different non-Gaussian TMST resource states. Gray (black) shaded region corresponds to $\Delta F^{\text{NG}} > 0$ with $F > 1/2$ ($F < 1/2$). We have taken $\kappa = 0.75$.

VI. CONCLUSION

In this study, we explored the significance of PS, PA, and PC operations on the TMST state in the context of quantum teleportation. Our findings demonstrate that these non-Gaussian operations can improve the performance of quantum teleportation. Additionally, our practical scheme allows us to factor in the success probability. When accounting for success probability, we observe that single PC and single PS operations prove to be optimal at low and intermediate squeezing levels for the quantum teleportation of input coherent states.

Our analysis addresses questions about whether the PC operation can enhance teleportation fidelity and how it compares with PS and PA operations. This analysis also helped answer the problem posed in Ref. [34] regarding the utility of the PCTMST state in quantum teleportation.

While TMSV states are more advantageous for quantum tasks, such states may not exist as pure states degrade to mixed states due to experimental imperfections and inevitable losses. The transformed mixed state is similar to the TMST state, rendering the analysis of TMST states important [3, 50–54].

The Wigner characteristic function for the non-Gaussian TMST states derived in this work is not available in the existing literature to the best of our knowledge. The introduction of this particular expression will serve as a valuable addition to the literature and

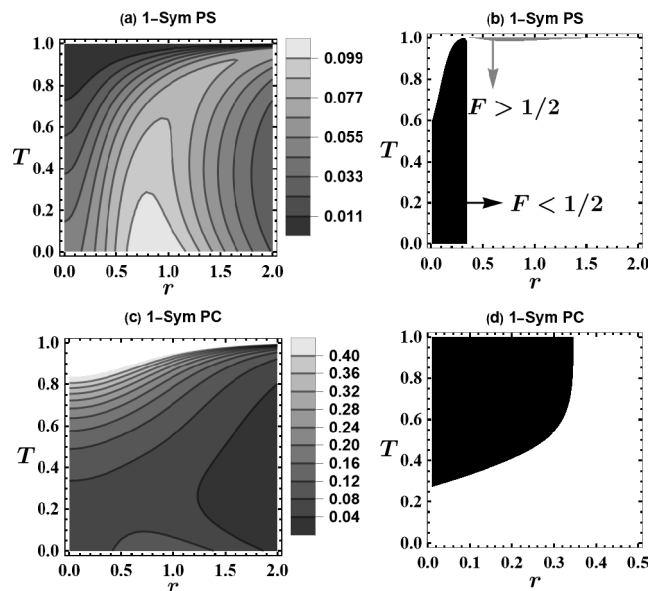


FIG. 14. First column: Success probability of different non-Gaussian operations on the TMST state. Second column: Fidelity enhancement ΔF^{NG} for the teleportation of input coherent states using different non-Gaussian TMST resource states. Gray (black) shaded region corresponds to $\Delta F^{\text{NG}} > 0$ with $F > 1/2$ ($F < 1/2$). We have taken $\kappa = 1$.

prove indispensable in the exploration of CV QIP protocols dealing with non-Gaussian TMST states. It will also be useful in the characterization of non-Gaussian TMST via quantifying nonlocality [55], steering [56], entanglement [57], non-Gaussianity [58, 59] and nonclassicality [60].

Appendix A: Phase space approach to CV systems

Our system of concern is a multi-mode system consisting of n non-interacting bosonic modes. The combined Hilbert space of such a system is given by the tensor product of the Hilbert spaces corresponding to the individual modes, $\mathcal{H}^{\otimes n} = \otimes_{i=1}^n \mathcal{H}_i$. Here, \mathcal{H}_i denotes the Hilbert space of the i^{th} mode. We represent the quadrature operators corresponding to the i^{th} mode of our system by \hat{q}_i and \hat{p}_i . Then the set of quadrature operators of our n -mode system can be written as [1, 2, 61–63]

$$\hat{\xi} = (\hat{\xi}_i) = (\hat{q}_1, \hat{p}_1, \dots, \hat{q}_n, \hat{p}_n)^T, \quad i = 1, 2, \dots, 2n. \quad (\text{A1})$$

The commutation relation between these quadrature operators can be expressed as (in natural units)

$$[\hat{\xi}_i, \hat{\xi}_j] = i\Omega_{ij}, \quad (i, j = 1, 2, \dots, 2n), \quad (\text{A2})$$

where

$$\Omega = \bigoplus_{k=1}^n \begin{pmatrix} 0 & 1 \\ -1 & 0 \end{pmatrix} \quad (\text{A3})$$

is the symplectic form on n modes.

Further, we define the photon annihilation operator for the i th mode as, $\hat{a}_i = \frac{1}{\sqrt{2}}(\hat{q}_i + i\hat{p}_i)$. In this article, two Gaussian operations namely, beam splitter operation $B_{ij}(T)$ and two mode squeezing operation $S_{ij}(r)$ is of special interest. The action of these Gaussian operations on the quadrature operators can be described through the following transformation matrices:

$$B_{ij}(T) : \begin{bmatrix} \hat{\xi}_i \\ \hat{\xi}_j \end{bmatrix} \mapsto \begin{bmatrix} \sqrt{T} \mathbb{1}_2 & \sqrt{1-T} \mathbb{1}_2 \\ -\sqrt{1-T} \mathbb{1}_2 & \sqrt{T} \mathbb{1}_2 \end{bmatrix} \begin{bmatrix} \hat{\xi}_i \\ \hat{\xi}_j \end{bmatrix}, \quad (\text{A4})$$

$$S_{ij}(r) : \begin{bmatrix} \hat{\xi}_i \\ \hat{\xi}_j \end{bmatrix} \mapsto \begin{bmatrix} \cosh r \mathbb{1}_2 & \sinh r \mathbb{Z} \\ \sinh r \mathbb{Z} & \cosh r \mathbb{1}_2 \end{bmatrix} \begin{bmatrix} \hat{\xi}_i \\ \hat{\xi}_j \end{bmatrix}, \quad (\text{A5})$$

where $\hat{\xi} = (\hat{q}_i, \hat{p}_i)^T$, $\mathbb{1}_2$ is the 2×2 identity matrix and $\mathbb{Z} = \text{diag}(1, -1)$. The TMST state is generated by applying the two mode squeezing operator on two uncorrelated thermal modes.

Now we introduce the Wigner characteristic function for representing a given density operator in the phase space formalism. The Wigner characteristic function of an n -mode CV system with density operator $\hat{\rho}$ is given by

$$\chi(\Lambda) = \text{Tr}[\hat{\rho} \exp(-i\Lambda^T \Omega \hat{\xi})], \quad (\text{A6})$$

where $\xi = (\hat{q}_1, \hat{p}_1, \dots, \hat{q}_n, \hat{p}_n)^T$, $\Lambda = (\Lambda_1, \Lambda_2, \dots, \Lambda_n)^T$ with $\Lambda_i = (\tau_i, \sigma_i)^T \in \mathcal{R}^2$.

It is worth noting that both the density operator formalism and the phase space approach using Wigner characteristic function are equivalent descriptions of CV systems. However in this article, we have exclusively used the latter for the sake of mathematical convenience.

For a single mode Fock state $|n\rangle$, the corresponding Wigner characteristic function can be obtained through Eq. (A6) and turns out to be:

$$\chi_{|n\rangle}(\tau, \sigma) = \exp\left[-\frac{\tau^2}{4} - \frac{\sigma^2}{4}\right] L_n\left(\frac{\tau^2}{2} + \frac{\sigma^2}{2}\right). \quad (\text{A7})$$

In the above equation, $L_n(x)$ is the Laguerre polynomial which belongs to the set of the classical orthogonal polynomials. The Laguerre polynomial in the above equation can be substituted with its corresponding generating function:

$$\chi_{|n\rangle}(\tau, \sigma) = \exp\left[-\frac{\tau^2}{4} - \frac{\sigma^2}{4}\right] \hat{F} e^{2st + s(\tau + i\sigma) - t(\tau - i\sigma)}, \quad (\text{A8})$$

with

$$\hat{F} = \frac{1}{2^n n!} \frac{\partial^n}{\partial s^n} \frac{\partial^n}{\partial t^n} \{\bullet\}_{s=t=0}. \quad (\text{A9})$$

The first order quadrature moments associated with our n -mode CV system described by the density operator $\hat{\rho}$ can be defined as

$$\mathbf{d} = \langle \hat{\xi} \rangle = \text{Tr}[\hat{\rho} \hat{\xi}]. \quad (\text{A10})$$

The second order quadrature moments can be represented in the form of the following matrix:

$$V = (V_{ij}) = \frac{1}{2} \langle \{\Delta \hat{\xi}_i, \Delta \hat{\xi}_j\} \rangle, \quad (\text{A11})$$

where $\Delta \hat{\xi}_i = \hat{\xi}_i - \langle \hat{\xi}_i \rangle$, and $\{, \}$ denotes anti-commutator. The above matrix, termed as covariance matrix, is a symmetric square matrix of order $2n$ with all of its entries real.

The states for which the quasi-probability distributions take on a Gaussian form are termed as Gaussian states. As a result, the characteristic functions corresponding to these distributions also turn out to be Gaussian as they are related to their corresponding distributions via a Fourier transform. These states are relatively simpler for analysis as their first and second order moments are sufficient to describe them. As stated earlier, in this article, we have utilized the Wigner characteristic function approach as it eases the mathematical complexity. We can write the Wigner characteristic function for a Gaussian state as follows [2, 64]:

$$\chi(\Lambda) = \exp\left[-\frac{1}{2} \Lambda^T (\Omega V \Omega^T) \Lambda - i(\Omega \mathbf{d})^T \Lambda\right]. \quad (\text{A12})$$

Here \mathbf{d} and V have their usual meanings as in Eqs. (A10) and (A11). The above equation can be used to obtain the Wigner characteristic function of a single mode coherent state:

$$\chi_{\text{coh}}(\Lambda) = \exp\left[-\frac{1}{4}(\tau^2 + \sigma^2) - i(\tau d_p - \sigma d_x)\right], \quad (\text{A13})$$

where d_x and d_p are related to the displacement vector as $\mathbf{d} = (d_x, d_p)^T$. Similarly, we can obtain the Wigner characteristic function of a single mode squeezed vacuum state with squeezing r from Eq. (A12):

$$\chi_{\text{sqv}}(\Lambda) = \exp\left[-\frac{1}{4}(\tau^2 e^{2r} + \sigma^2 e^{-2r})\right]. \quad (\text{A14})$$

Consider our system of interest being subjected to a symplectic transformation S . The state of our system represented by the density operator $\hat{\rho}$ will then change to $\rho \rightarrow \mathcal{U}(S) \hat{\rho} \mathcal{U}(S)^\dagger$, where $\mathcal{U}(S)$ is the infinite dimensional unitary operator corresponding to the symplectic transformation S . Under the symplectic transformation S , the first and second moments transform as $\mathbf{d} \rightarrow S\mathbf{d}$ and $V \rightarrow SVS^T$, respectively. The Wigner characteristic function changes from $\chi(\Lambda)$ to $\chi(S^{-1}\Lambda)$.

Appendix B: Matrices

$$M_1 = \frac{-1}{4a_0} \begin{pmatrix} a_1 & 0 & a_2 & 0 \\ 0 & a_1 & 0 & -a_2 \\ a_2 & 0 & a_3 & 0 \\ 0 & -a_2 & 0 & a_3 \end{pmatrix}, \quad (\text{B1})$$

where

$$\begin{aligned}
a_0 &= 4\kappa^2 r_1^2 r_2^2 + \gamma (1 - t_1^2 t_2^2) + \Gamma_1 \Gamma_2 \\
a_1 &= 4\Gamma_1 \kappa^2 r_2^2 + \gamma (1 + t_1^2 t_2^2) + \Gamma_2 r_1^2 \\
a_2 &= -16\alpha\beta\kappa t_1 t_2 \\
a_3 &= 4\Gamma_2 \kappa^2 r_1^2 + \gamma (1 + t_1^2 t_2^2) + \Gamma_1 r_2^2
\end{aligned} \tag{B2}$$

Here $\Gamma_i = (1 + T_i)$, $t_i = \sqrt{T_i}$, and $r_i = \sqrt{1 - T_i}$ ($i = 1, 2$). Further $\alpha = \sinh r$, $\beta = \cosh r$, and $\gamma = 4\kappa(\alpha^2 + \beta^2)$.

$$M_2 = \frac{1}{a_0} \begin{pmatrix} b_1 & ib_1 & b_2 & -ib_2 \\ b_3 & ib_1 & -b_2 & -ib_2 \\ b_4 & -ib_4 & b_5 & ib_5 \\ -b_4 & -ib_4 & b_6 & ib_5 \\ b_7 & ib_7 & b_8 & -ib_8 \\ -b_7 & ib_7 & -b_8 & -ib_8 \\ b_9 & -ib_9 & b_{10} & ib_{10} \\ -b_9 & -ib_9 & -b_{10} & ib_{10} \end{pmatrix}, \tag{B3}$$

where

$$\begin{aligned}
b_1 &= r_1 (\gamma + \Gamma_2 + 4\kappa^2 r_2^2) \\
b_2 &= -8\alpha\beta\kappa r_1 t_1 t_2 \\
b_3 &= -r_1 (\gamma + \Gamma_2 + 4\kappa^2 r_2^2) \\
b_4 &= -8\alpha\beta\kappa r_2 t_1 t_2 \\
b_5 &= r_2 (\gamma + \Gamma_1 + 4\kappa^2 r_1^2) \\
b_6 &= -r_2 (\gamma + \Gamma_1 + 4\kappa^2 r_1^2) \\
b_7 &= r_1 t_1 (\Gamma_2 + 4\kappa^2 r_2^2 - \gamma t_2^2) \\
b_8 &= 8\alpha\beta\kappa r_1 t_2 \\
b_9 &= 8\alpha\beta\kappa r_2 t_1 \\
b_{10} &= r_2 t_2 (\Gamma_1 + 4\kappa^2 r_1^2 - \gamma t_1^2)
\end{aligned} \tag{B4}$$

$$M_3 = \frac{1}{a_0} \begin{pmatrix} 0 & c_1 & c_2 & 0 & 0 & c_3 & c_4 & 0 \\ c_1 & 0 & 0 & c_2 & c_3 & 0 & 0 & c_4 \\ c_2 & 0 & 0 & c_5 & c_6 & 0 & 0 & c_7 \\ 0 & c_2 & c_5 & 0 & 0 & c_6 & c_7 & 0 \\ 0 & c_3 & c_6 & 0 & 0 & c_8 & c_9 & 0 \\ c_3 & 0 & 0 & c_6 & c_8 & 0 & 0 & c_9 \\ c_4 & 0 & 0 & c_7 & c_9 & 0 & 0 & c_{10} \\ 0 & c_4 & c_7 & 0 & 0 & c_9 & c_{10} & 0 \end{pmatrix} \tag{B5}$$

where

$$\begin{aligned}
c_1 &= r_1^2 (\gamma + \Gamma_2 + 4\kappa^2 r_2^2) \\
c_2 &= 8\alpha\beta\kappa r_1 r_2 t_1 t_2 \\
c_3 &= t_1 (2\Gamma_2 + \gamma r_2^2) \\
c_4 &= -8\alpha\beta\kappa r_1 r_2 t_1 \\
c_5 &= r_2^2 (\gamma + \Gamma_1 + 4\kappa^2 r_1^2) \\
c_6 &= -8\alpha\beta\kappa r_1 r_2 t_2 \\
c_7 &= t_2 (2\Gamma_1 + \gamma r_1^2) \\
c_8 &= r_1^2 (-\Gamma_2 + 4\kappa^2 r_2^2 + \gamma t_2^2) \\
c_9 &= 8\alpha\beta\kappa r_1 r_2 \\
c_{10} &= r_2^2 (-\Gamma_1 + 4\kappa^2 r_1^2 + \gamma t_1^2)
\end{aligned} \tag{B6}$$

-
- [1] S. L. Braunstein and P. van Loock, Quantum information with continuous variables, *Rev. Mod. Phys.* **77**, 513 (2005).
- [2] C. Weedbrook, S. Pirandola, R. García-Patrón, N. J. Cerf, T. C. Ralph, J. H. Shapiro, and S. Lloyd, Gaussian quantum information, *Rev. Mod. Phys.* **84**, 621 (2012).
- [3] N. Takei, T. Aoki, S. Koike, K.-i. Yoshino, K. Wakui, H. Yonezawa, T. Hiraoka, J. Mizuno, M. Takeoka, M. Ban, and A. Furusawa, Experimental demonstration of quantum teleportation of a squeezed state, *Phys. Rev. A* **72**, 042304 (2005).
- [4] M. S. Kim, F. A. M. de Oliveira, and P. L. Knight, Properties of squeezed number states and squeezed thermal states, *Phys. Rev. A* **40**, 2494 (1989).
- [5] R. Chrapkiewicz, Photon counts statistics of squeezed and multimode thermal states of light on multiplexed on-off detectors, *J. Opt. Soc. Am. B* **31**, B8 (2014).
- [6] E. Fitzke, F. Niederschuh, and T. Walther, Simulating the photon statistics of multimode Gaussian states by automatic differentiation of generating functions, *APL Photonics* **8**, 10.1063/5.0129638 (2023), 026106.
- [7] P. Marian, Higher-order squeezing and photon statistics for squeezed thermal states, *Phys. Rev. A* **45**, 2044 (1992).
- [8] P. Marian, T. A. Marian, and H. Scutaru, Bures distance as a measure of entanglement for two-mode squeezed thermal states, *Phys. Rev. A* **68**, 062309 (2003).
- [9] S. Cialdi, C. Porto, D. Cipriani, S. Olivares, and M. G. A. Paris, Full quantum state reconstruction of symmetric two-mode squeezed thermal states via spectral homodyne detection and a state-balancing detector, *Phys. Rev. A* **93**, 043805 (2016).
- [10] D. Afshar, F. Abbasnezhad, S. Mehrabankar, and A. Isar, Two-mode gaussian states as resource of secure quantum teleportation in open systems, *Chinese Journal of Physics* **68**, 419 (2020).
- [11] J. Yu, Y. Qin, J. Qin, H. Wang, Z. Yan, X. Jia, and K. Peng, Quantum enhanced optical phase estimation with a squeezed thermal state, *Phys. Rev. Appl.* **13**, 024037 (2020).
- [12] Q.-S. Tan, J.-Q. Liao, X. Wang, and F. Nori, Enhanced interferometry using squeezed thermal states and even or odd states, *Phys. Rev. A* **89**, 053822 (2014).
- [13] H.-M. Li, X.-X. Xu, H.-C. Yuan, and Z. Wang, Quantum metrology with two-mode squeezed thermal state: Parity detection and phase sensitivity, *Chinese Physics B* **25**, 104203 (2016).
- [14] M. Cuzminschi, A. Zubarev, and A. Isar, Extractable quantum work from a two-mode gaussian state in a noisy channel, *Scientific Reports* **11**, 24286 (2021).
- [15] R. Birrittella, J. Mimih, and C. C. Gerry, Multiphoton quantum interference at a beam splitter and the approach to heisenberg-limited interferometry, *Phys. Rev. A* **86**, 063828 (2012).
- [16] R. Carranza and C. C. Gerry, Photon-subtracted two-mode squeezed vacuum states and applications to quantum optical interferometry, *J. Opt. Soc. Am. B* **29**, 2581 (2012).
- [17] D. Braun, P. Jian, O. Pinel, and N. Treps, Precision measurements with photon-subtracted or photon-added gaussian states, *Phys. Rev. A* **90**, 013821 (2014).
- [18] Y. Ouyang, S. Wang, and L. Zhang, Quantum optical interferometry via the photon-added two-mode squeezed vacuum states, *J. Opt. Soc. Am. B* **33**, 1373 (2016).
- [19] H. Zhang, W. Ye, C. Wei, Y. Xia, S. Chang, Z. Liao, and L. Hu, Improved phase sensitivity in a quantum optical interferometer based on multiphoton catalytic two-mode squeezed vacuum states, *Phys. Rev. A* **103**, 013705 (2021).
- [20] C. Kumar, Rishabh, and S. Arora, Realistic non-gaussian-operation scheme in parity-detection-based mach-zehnder quantum interferometry, *Phys. Rev. A* **105**, 052437 (2022).
- [21] M. Verma, C. Kumar, K. K. Mishra, and P. K. Panigrahi, Optimal non-gaussian operations in difference-intensity detection and parity detection-based mach-zehnder interferometer, arXiv preprint arXiv:2312.10774 (2023).
- [22] T. Opatrný, G. Kurizki, and D.-G. Welsch, Improvement on teleportation of continuous variables by photon subtraction via conditional measurement, *Phys. Rev. A* **61**, 032302 (2000).
- [23] Y. Yang and F.-L. Li, Entanglement properties of non-gaussian resources generated via photon subtraction and addition and continuous-variable quantum-teleportation improvement, *Phys. Rev. A* **80**, 022315 (2009).
- [24] X.-x. Xu, Enhancing quantum entanglement and quantum teleportation for two-mode squeezed vacuum state by local quantum-optical catalysis, *Phys. Rev. A* **92**, 012318 (2015).
- [25] L. Hu, Z. Liao, and M. S. Zubairy, Continuous-variable entanglement via multiphoton catalysis, *Phys. Rev. A* **95**, 012310 (2017).
- [26] S. Wang, L.-L. Hou, X.-F. Chen, and X.-F. Xu, Continuous-variable quantum teleportation with non-gaussian entangled states generated via multiple-photon subtraction and addition, *Phys. Rev. A* **91**, 063832 (2015).
- [27] C. Kumar and S. Arora, Success probability and performance optimization in non-gaussian continuous-variable quantum teleportation, *Phys. Rev. A* **107**, 012418 (2023).
- [28] C. Kumar, M. Sharma, and S. Arora, Continuous variable quantum teleportation in a dissipative environment: Comparison of non-gaussian operations before and after noisy channel, *Advanced Quantum Technologies* **n/a**, 2300344.
- [29] S.-Y. Lee, S.-W. Ji, H.-J. Kim, and H. Nha, Enhancing quantum entanglement for continuous variables by a coherent superposition of photon subtraction and addition, *Phys. Rev. A* **84**, 012302 (2011).
- [30] M. S. Kim, H. Jeong, A. Zavatta, V. Parigi, and M. Bellini, Scheme for proving the bosonic commutation relation using single-photon interference, *Phys. Rev. Lett.* **101**, 260401 (2008).
- [31] H. S. Dhar, A. Chatterjee, and R. Ghosh, Generating continuous variable entangled states for quantum teleportation using a superposition of number-conserving operations, *Journal of Physics B: Atomic, Molecular and Optical Physics* **48**, 185502 (2015).
- [32] H. Zhang, W. Ye, C. Wei, C. Liu, Z. Liao, and L. Hu, Improving phase estimation using number-conserving operations, *Phys. Rev. A* **103**, 052602 (2021).

- [33] H.-L. Zhang, Y.-Q. Hu, F. Jia, and L.-Y. Hu, Entanglement of photon-subtracted two-mode squeezed thermal state and its decoherence in thermal environments, *International Journal of Theoretical Physics* **53**, 2091 (2014).
- [34] X.-G. Meng, K.-C. Li, J.-S. Wang, X.-Y. Zhang, Z.-T. Zhang, Z.-S. Yang, and B.-L. Liang, Continuous-variable entanglement and wigner-function negativity via adding or subtracting photons, *Annalen der Physik* **532**, 1900585 (2020).
- [35] L.-Y. Hu, F. Jia, and Z.-M. Zhang, Entanglement and nonclassicality of photon-added two-mode squeezed thermal state, *J. Opt. Soc. Am. B* **29**, 1456 (2012).
- [36] A. I. Lvovsky, H. Hansen, T. Aichele, O. Benson, J. Mlynek, and S. Schiller, Quantum state reconstruction of the single-photon fock state, *Phys. Rev. Lett.* **87**, 050402 (2001).
- [37] A. Zavatta, S. Viciani, and M. Bellini, Tomographic reconstruction of the single-photon fock state by high-frequency homodyne detection, *Phys. Rev. A* **70**, 053821 (2004).
- [38] S. R. Huisman, N. Jain, S. A. Babichev, F. Vewinger, A. N. Zhang, S. H. Youn, and A. I. Lvovsky, Instant single-photon fock state tomography, *Opt. Lett.* **34**, 2739 (2009).
- [39] A. Ourjoumtsev, R. Tualle-Brouiri, and P. Grangier, Quantum homodyne tomography of a two-photon fock state, *Phys. Rev. Lett.* **96**, 213601 (2006).
- [40] M. Cooper, L. J. Wright, C. Söller, and B. J. Smith, Experimental generation of multi-photon fock states, *Opt. Express* **21**, 5309 (2013).
- [41] A. E. Lita, A. J. Miller, and S. W. Nam, Counting near-infrared single-photons with 95% efficiency, *Opt. Express* **16**, 3032 (2008).
- [42] F. Marsili, V. B. Verma, J. A. Stern, S. Harrington, A. E. Lita, T. Gerrits, I. Vayshenker, B. Baek, M. D. Shaw, R. P. Mirin, and S. W. Nam, Detecting single infrared photons with 93% system efficiency, *Nature Photonics* **7**, 210 (2013).
- [43] I. Esmaeil Zadeh, J. W. N. Los, R. B. M. Gourgues, V. Steinmetz, G. Bulgarini, S. M. Dobrovolskiy, V. Zwiller, and S. N. Dorenbos, Single-photon detectors combining high efficiency, high detection rates, and ultra-high timing resolution, *APL Photonics* **2**, 111301 (2017).
- [44] S. L. Braunstein and H. J. Kimble, Teleportation of continuous quantum variables, *Phys. Rev. Lett.* **80**, 869 (1998).
- [45] S. L. Braunstein, C. A. Fuchs, and H. J. Kimble, Criteria for continuous-variable quantum teleportation, *Journal of Modern Optics* **47**, 267 (2000).
- [46] S. L. Braunstein, C. A. Fuchs, H. J. Kimble, and P. van Loock, Quantum versus classical domains for teleportation with continuous variables, *Phys. Rev. A* **64**, 022321 (2001).
- [47] H. Vahlbruch, M. Mehmet, K. Danzmann, and R. Schnabel, Detection of 15 db squeezed states of light and their application for the absolute calibration of photoelectric quantum efficiency, *Phys. Rev. Lett.* **117**, 110801 (2016).
- [48] O. S. Magaña-Loaiza, R. d. J. León-Montiel, A. Perez-Leija, A. B. U'Ren, C. You, K. Busch, A. E. Lita, S. W. Nam, R. P. Mirin, and T. Gerrits, Multiphoton quantum-state engineering using conditional measurements, *npj Quantum Information* **5**, 80 (2019).
- [49] O. Rosas-Ortiz and K. Zelaya, Theory of photon subtraction for two-mode entangled light beams, *Quantum Reports* **3**, 500 (2021).
- [50] M. Aspachs, J. Calsamiglia, R. Muñoz Tapia, and E. Bagan, Phase estimation for thermal gaussian states, *Phys. Rev. A* **79**, 033834 (2009).
- [51] S. Pirandola, G. Spedalieri, S. L. Braunstein, N. J. Cerf, and S. Lloyd, Optimality of gaussian discord, *Phys. Rev. Lett.* **113**, 140405 (2014).
- [52] Y. Xiang, B. Xu, L. Mišta, T. Tufarelli, Q. He, and G. Adesso, Investigating einstein-podolsky-rosen steering of continuous-variable bipartite states by non-gaussian pseudospin measurements, *Phys. Rev. A* **96**, 042326 (2017).
- [53] C. Vendromin and M. M. Dignam, Continuous-variable entanglement in a two-mode lossy cavity: An analytic solution, *Phys. Rev. A* **103**, 022418 (2021).
- [54] C. Kumar, Rishabh, and S. Arora, Enhanced phase estimation in parity-detection-based mach-zehnder interferometer using non-gaussian two-mode squeezed thermal input state, *Annalen der Physik* **535**, 2300117 (2023).
- [55] C. Kumar, G. Saxena, and Arvind, Continuous-variable clauser-horne bell-type inequality: A tool to unearth the nonlocality of continuous-variable quantum-optical systems, *Phys. Rev. A* **103**, 042224 (2021).
- [56] P. Chowdhury, T. Pramanik, A. S. Majumdar, and G. S. Agarwal, Einstein-podolsky-rosen steering using quantum correlations in non-gaussian entangled states, *Phys. Rev. A* **89**, 012104 (2014).
- [57] M. Allegra, P. Giorda, and M. G. A. Paris, Role of initial entanglement and non-gaussianity in the decoherence of photon-number entangled states evolving in a noisy channel, *Phys. Rev. Lett.* **105**, 100503 (2010).
- [58] J. S. Ivan, M. S. Kumar, and R. Simon, A measure of non-gaussianity for quantum states, *Quantum Information Processing* **11**, 853 (2012).
- [59] J. Park, J. Lee, K. Baek, and H. Nha, Quantifying non-gaussianity of a quantum state by the negative entropy of quadrature distributions, *Phys. Rev. A* **104**, 032415 (2021).
- [60] W. Ge and M. S. Zubairy, Evaluating single-mode non-classicality, *Phys. Rev. A* **102**, 043703 (2020).
- [61] Arvind, B. Dutta, N. Mukunda, and R. Simon, The real symplectic groups in quantum mechanics and optics, *Pramana* **45**, 471 (1995).
- [62] G. Adesso and F. Illuminati, Entanglement in continuous-variable systems: recent advances and current perspectives, *J. Phys. A* **40**, 7821 (2007).
- [63] G. Adesso, S. Ragy, and A. R. Lee, Continuous variable quantum information: Gaussian states and beyond, *Open Syst. Inf. Dyn.* **21**, 1440001, 47 (2014).
- [64] S. Olivares, Quantum optics in the phase space, *The European Physical Journal Special Topics* **203**, 3 (2012).